Desalination and Water Treatment
www.deswater.com
doi: 10.5004/dwt.2022.28189

250 (2022) 221–239
February

Paroxysmal black water events in reservoirs: the case of Tianbao Reservoir, China

Robert Bofah-Buoh[a], Yiping Li[a,*], Ya Zhu[a], Patrick Banahene[a], Linda Akosua Nuamah[a], Eyram Norgbey[a], Williams Kweku Darkwah[b]

[a]*Key Laboratory of Integrated Regulation and Resources Development of Shallow Lakes of Ministry of Education, College of Environment, Hohai University, Nanjing 210098, China, Tel. +8613813966025; emails: liyiping@hhu.edu.cn (Y. Li), lanimap12@yahoo.com (R. Bofah-Buoh), 836674553@qq.com (Y. Zhu), ghbanahene@yahoo.com (P. Banahene), nuamahlinda@yahoo.com (L.A. Nuamah), eyramn@hhu.edu.cn (E. Norgbey)*
[b]*School of Chemical Engineering, Faculty of Engineering, UNSW Sydney, 2052 NSW, Sydney, Australia, email: williamsdarkwakwaku@yahoo.com (W.K. Darkwah)*

Received 27 October 2021; Accepted 12 January 2022

ABSTRACT

Iron (Fe), manganese (Mn), sulfide (S), organic matter (OM) and *Eucalyptus* sp. have direct and indirect influences on reservoir water quality and the aquatic environment. In this study, a 35-days of the field study was conducted using the diffusive gradients in thin films (DGT) and the planar optode to address the unknown combined effects of Fe, Mn, OM and tannins from *Eucalyptus* sp. on Tianbao Reservoir. Our results indicated that the hypolimnion was hypoxic due to thermal stratification, which caused the reduction of insoluble Fe and Mn from sediments to benthic water. Thermal stratification was severe on day 1 and was destroyed on day 35. The hypoxia added greatly to the elevated positive fluxes (Fe^{2+}, Mn^{2+}, S^{2-}) measured on day 1. Black substances (iron sulfide and manganese sulfide) were formed in the benthic region. Substantial decrease ($p < 0.05$) in the content of Fe^{2+}, tannins and dissolved organic carbon (DOC) (overlying water) from days 1 to 35 revealed that these elements reacted to form black substances. The DIFS model showed that the remobilization of Fe^{2+} was the non-steady-state case of "partially sustained" category from days 1 to 35. Thus, the utilization of the DGT and DIFS model is an excellent way to comprehend the generation of black water in reservoirs. The variability in the fluxes and concentration of Fe and DOC at the sediment-water boundary due to changes in oxygen and redox conditions provides useful information on how to improve the quality of freshwater management designs.

Keywords: Diffusive gradient in thin films; DIFS model; Planar optode; Black water; HR-peeper

1. Introduction

Reservoirs across the world are vital to the ecosystem. Reservoirs are of utmost importance since they provide services such as water supply for domestic and industrial use, irrigational use, generation of electricity, flood control purposes and urbanization [1]. Presently, the pollution of reservoirs due to iron (Fe) and manganese (Mn) has become an alarming concern across the world [2]. A high concentration of Fe and Mn influences the taste and colour of reservoir drinking water [3], posing as a severe threat to human health. Health issues like neurobehavioral effects, liver cancer, respiratory, reproductive, renal damage, immunological, mutagenic effects, and gastrointestinal toxicity have resulted from the consumption of water with high Fe and Mn concentrations. Thus, it is imperative to study the management of Fe and Mn in reservoir and its water quality assessment.

* Corresponding author.

1944-3994/1944-3986 © 2022 Desalination Publications. All rights reserved.

The variability of Fe and Mn in reservoirs is strongly affected by the distribution of dissolved oxygen (DO) concentration in the water column [4]. The water density and oxygen content at varying reservoir depths are influenced by thermal stratification. The water columns mix, and oxygen finds its way to the bottom water when the stratification is weak. The thermocline thickness is huge when stratification is intensified, hence stopping the water column from mixing. When the hypolimnion is oxic (low/no thermal stratification), Fe and Mn exist in their oxidized forms (Fe and Mn oxyhydroxides) at the sediment-water boundary (SWB). On the other hand, when the hypolimnion is hypoxic (DO concentration is more significant than 2 mg L^{-1}) during intense stratification, Fe and Mn are reduced at the SWB. This causes the release of soluble Fe and Mn from sediments to bottom (benthic) water [5]. Water degradation in reservoirs (due to Fe and Mn) adversely affects the ecology of the aquatic environment by decreasing aquatic organisms' productivity [6]. In addition to water degradation in reservoirs due to Fe and Mn, much attention also needs to be given to pollution caused by *Eucalyptus* sp. leaves. *Eucalyptus* sp. native to Australia [7], can be found in more than 120 countries because of its high economic value, wide adaptability, and rapid growth rate [7]. In China, the area covered by the *Eucalyptus* sp. plantations is more than 4 million hm^2 [9]. Although the tree has many advantages, there are a few concerns raised due to the planting of *Eucalyptus* sp. trees. The leaves contain a high amount of tannic acid and are washed into the reservoir (via wind and rainfall). This affects the reservoir water quality [10,11]. Black water phenomenon which occurs in Southern China water systems is because of the complexation reaction between Fe and tannins from *Eucalyptus* sp. trees. This phenomenon has contributed to the profound negative impact on aquatic system processes and functions such as the depopulation of marine organisms [10]. Fe and Mn further contribute to black water formation in reservoirs by co-precipitating with sulfide (S) in an oxygen deficient environment to form black precipitates (FeS and MnS) [12]. Thus, it is imperative to study interactions between Fe, Mn, and *Eucalyptus* sp. trees during hypoxia to understand their impact on reservoir water quality.

In this study, we hypothesized that the formation of black in the reservoirs (during winter) in Southern China was due to interaction between iron (Fe^{2+}) and tannins from *Eucalyptus* sp. when the water column mixes (thermal stratification ceases). To confirm this hypothesis, we carried out field investigations using high-resolution (millimetre scale) technique to understand the mechanistic pathway leading to reservoir water degradation (black water).

The diffusive gradients in thin films (DGT), planar optode and high-resolution peeper were employed to determine the synergistic effect of Fe, Mn, and *Eucalyptus* sp. in deteriorating the water quality of Tianbao Reservoir. The DGT device provides useful information on speciation and bioavailability of trace metals compared to traditional methods [13]. Furthermore, the remobilization and resupply ability of trace metals at the SWB can be explored into details using the Diffusive gradient technology and DIFS model [14]. The yellow spring instrument water quality parameter device was attached a high-frequency buoy to measure the variation in oxidation–reduction potential (ORP) and pH in the hypolimnion on a daily and hourly scale. The Planar Optrode provided clear information in 2D at the SWB on hypoxia variation. Thus, in this study, we used DGT, HR-peeper, PO, YSI, DIFS model to unravel the release risk and effects of Fe^{2+}, Mn^{2+} and *Eucalyptus* sp. leaves (tannins) on the reservoir. Generally, most studies on water quality deterioration (black water due to Fe, Mn, and *Eucalyptus* plantation) focused on shallow water systems (rivers, ponds and lakes) with few studies conducted in relatively deep reservoirs. In this research work, a 35-days field investigation was conducted to unravel the drivers responsible for the water degradation in reservoirs. Thus, the Tianbao Reservoir in Southern China was investigated to:

- study the concentration and kinetics of Fe, Mn, and S to understand their resupply kinetics, flux and remobilization characteristics;
- study the variation in oxygen distribution (hypoxia) with the aid of the planar optode to understand the role hypoxia plays in black water development in the reservoir;
- understand how tannins from *Eucalyptus* sp. can interact with Fe to form black water in the reservoir;
- understand how changes in the thermal structure of the reservoir contribute to black water formation in the reservoir;

Until now, no such exploration has not been carried out on reservoirs on a daily scale. Thus, this work constitutes a first quantitative attempt to examine combined effects of Fe, Mn and *Eucalyptus* sp. leave on reservoir water quality using a high-resolution and high-frequency approach on a daily scale.

2. Materials and methodology

2.1. Study design

The study approach was in fourfold. First, the water quality properties of the reservoir were determined. Second, we used the DGT and HR-peeper technique to understand resupply kinetics and flux characteristics of iron, manganese, and sulfide. Third, we conducted a 35-days field investigation to monitor the changes of Fe^{2+}, tannins, dissolved organic carbon (DOC) (*Eucalyptus* sp.), oxygen content and thermal structure at the SWB of the reservoir. Fourth, the DIFS model investigated the remobilization of Fe^{2+} ions. These steps are described in more detail in the following sections.

2.2. Site description

The study site (22° 52′ 15.84″ – 22° 53′ 16.51″N, 108°12′ 32″ – 108°14′ 10″E) is in Nanning City of Guangxi Province, Southern China (Fig. 1). The *Eucalyptus* trees are prevalent around the reservoir in Southern China and occupy more than 65% of the total catchment area of the Tianbao Reservoir [14]. For over 10 y, there has been cutting of *Eucalyptus* trees in the research area. Thermal stratification for Tianbao Reservoirs is from April to November, where the

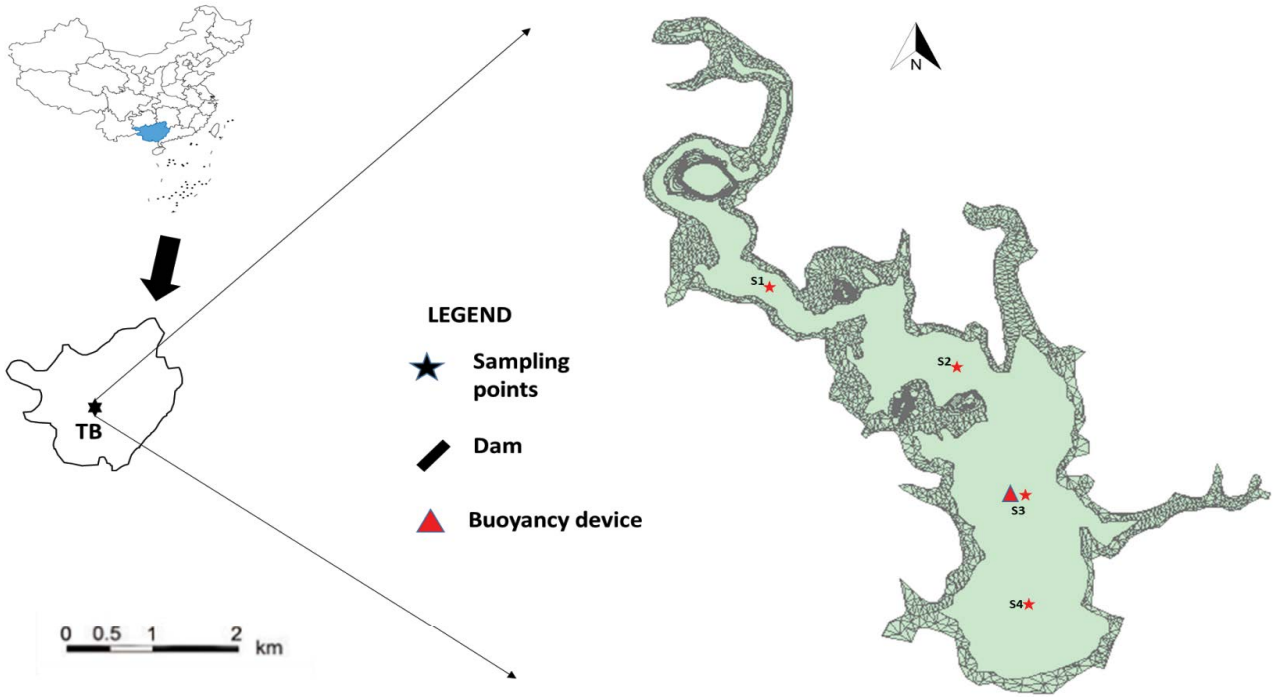

Fig. 1. Map of the study area.

bottom water has little or no oxygen [4]. During the mixing period in early December, the water in the reservoir changes to black during which the thermal structure of the reservoir is destroyed.

Four sites (S1 to S4) were investigated in November–December 2019 (Fig. 1). S1 and S2 have a sampling depth of 8.5 m, while S3 and S4 have a sampling depth of about 12 m. The water samples collected in the reservoir at different depths were divided into two layers (i.e., upper, and bottom depth). The upper and bottom layers for S1/S2 was 0–5 m and 5–8.5 m respectively while that of S3/S4 was 0–7 m and 7–12 m, respectively.

2.3. Sampling and chemical analysis of water column

The water temperature and oxygen content in the reservoir, as well as the pH and reduction potential were measured with the aid of YSI (Yellow Springs Instruments EXO_2) purchased from YSI Corporation, Yellow Springs, OH, USA. The sampling was done in the reservoir water column at an interval of 0.5 m on November 22 (day 1) to December 23, 2019 (day 32). The water samples were collected at intervals of 1 m using Plexiglass hydrophore water sample collector (purchased from the Guangxi Water Research Centre, China) for the determination of total iron, total manganese, dissolved (soluble) organic carbon (DOC) and tannins. The collected water samples were stored in polyethylene water storage container with a volume of 500 mL. For temporary storage, 1.0 mL of nitric acid was added to the water sample for the testing of Fe and Mn. For sulfide, 1 mL of sodium hydroxide was added to the water sample while no reagent was added to water samples for the testing of DOC. After collection, the water samples were stored in a fridge at 4°C. Measuring of total iron and manganese was performed using the Perkin Elmer Optima 8300 ICP-OES (Inductively Coupled Plasma-Optical Emission Spectrometry), Winston-Salem, USA [3]. DOC was analysed using the combustion infrared technique [16], and sulfide was tested using the blue methylene spectrophotometer technique [17]. The tannins content was measured using the ultraviolet spectrophotometer technique [18].

2.4. DGT, HR-peeper and DGT-DIFS model technique

2.4.1. Usage of DGT and HR-peeper

The UWITEC core sampler (EasySensor Institute, China) was used for sediment sampling (Fig. 1). Sampling was done from November 22 (day 1) to December 23, 2019 (day 32). The collected samples were stored for 24 h before deploying the DGT and HR-peeper (millimeter scale) device. The EasySensor Company in Nanjing, China, provided the millimeter scale devices for the experiment. In this study, the amount of labile-Fe^{2+} and labile-S^{2-} at the SWB were investigated using the ZrO-Chelex DGT and the AgI DGT devices, respectively [4]. The HR-peeper was used to determine the dissolved soluble Mn^{2+}, Fe^{2+} and DOC. The concentration, measured by the HR-peeper, is the hypothetical sediment pore water concentration of the trace metal [13].

2.4.2. DGT and HR-peeper deployment and analysis

The complete guide about the usage of DGT and HR-peeper devices has been previously discussed in our work [4] and has been briefly presented here. The sediment samples were allowed to settle for 24 h after sample

collection. First, the HR-peeper was driven into the sample. Second, the DGT device was inserted after 24 h of placing the HR-peeper device into the sediment column. The DGT and HR-peeper were then removed and cleaned [4]. The concentrations of labile Fe were measured with the Epoch Microplate Spectrophotometer equipment. The content of Fe^{2+} in the pore water (HR-peeper device) was acidized with HNO_3 to prevent Fe(II) oxidation [19]. Ferrous Fe (Fe^{2+}) was measured using the phenanthroline colorimetric method [20]. Mn^{2+} concentration was measured using the spectrophotometric method [21]. The ultraviolet photo-oxidation technique was used to measure the content of DOC in the samples. Measurement of standard solutions was assured by the analytical quality control (QC) for Fe^{2+} and Mn^{2+}. From the testing findings, a high correlation ($r^2 > 0.8$) was obtained. The standard deviations (relative) were 4.7% and 4.1%, for Fe^{2+} and Mn^{2+} respectively.

2.4.3. DGT content measurement

The amount of Fe^{2+} and S^{2-} was calculated according to Eq. (1) [17].

$$C_{DGT} = \frac{M\Delta g}{DAt} \tag{1}$$

where C_{DGT} is measured based on the mass M (ng) collected on the binding gel; g (cm) layer thickness (diffusive gel, membrane filter and diffusive path length), D ($cm^2\ s^{-1}$) the target analyte's diffusion coefficient; t (s) deployment duration; A (cm^2) sampling window's area.

2.4.4. Flux measurement at SWB

The net flux at the SWB was measured following Eq. (2):

$$F = F_W + F_S = -D_W\left(\frac{\partial C_{DGT}}{\partial X_W}\right)_{(x=0)} - \varphi D_S\left(\frac{\partial C_{DGT}}{\partial X_S}\right)_{(x=0)} \tag{2}$$

where F ($g\ cm^{-2}\ s^{-1}$) is the net flux measured at the SWB. F_W ($g\ cm^{-2}\ s^{-1}$) and F_S ($g\ cm^{-2}\ s^{-1}$) are labile fluxes (Fe^{2+}, Mn^{2+} S^{2-}) from benthic water to SWB and from sediment to SWB, respectively. $\left(\partial C_{DGT} / \partial X_W\right)_{(x=0)}$ and $\left(\partial C_{DGT} / \partial X_S\right)_{(x=0)}$ are concentration (labile) gradient in benthic water and sediment respectively. D_S ($cm^2\ s^{-1}$) and D_W ($cm^2\ s^{-1}$) are element's diffusion coefficients in sediment and benthic water respectively. Φ is the sediment's porosity.

Gradient distance (at SWB) is 10 mm [4,12]. The porosity was determined following a study by Tamura et al. [20] [Eq. (3)].

$$\Phi = \frac{Wd_s}{(1-W)d_w + Wd_s} \tag{3}$$

where W refers to water content in sediment; d_s and d_w are the mean density of sediment and benthic water.

2.4.5. DIFS model

The DIFS model investigated the remobilization of iron (Fe^{2+}) at the SWB. The parameters of the model are presented in this research work (Table 1). The parameters were computed following Eqs. (4)–(11) [14]. The detailed guide for

Table 1
The definitions of the DIFS model parameters

Parameter	Definition	Input/Output
C_{DGT}, mg L^{-1}	DGT concentration	Input
C_s, mol g^{-1}	Solid-phase's available concentration	Input
C_{peeper} (C_{sol}), mg L^{-1}	Dissolved/soluble concentration	Input
R	Ratio of DGT concentration to soluble concentration	Input
K_d, $cm^3\ g^{-1}$	Distribution (equilibrium) coefficient between pore water and solid-phase	Input
P_c, g cm^{-3}	Particle concentration	Input
ϕ_d	Porosity of diffusion layer	Input
ϕ_s	Porosity of sediment	Input
D_o, $cm^2\ s^{-1}$	Coefficients of diffusion layer	Input
D_S, $cm^2\ s^{-1}$	Sediment's diffusion coefficients	Input
T, h	Time of deployment	Input
Δg, cm	Thickness of diffusion layer	Input
T_c, s	(De)sorption process's response time	Output
K_1, s^{-1}	Rate constant of sorption	Output
K_{-1}, s^{-1}	Rate constant of desorption	Output
C_o, mol cm^{-3}	Gap water's concentration	Input
H_1, mg g^{-1}	Acid-soluble/exchangeable fraction of Fe	Input
W_0, g	Mass of wet sediment	Input
W_1, g	Mass of the sediment after drying at 105	Input
ρ, g cm^{-3}	Density of the water	Input

the usage of the DGT-DIFS model has been provided in supplementary Fig. S1.

$$P_c = \frac{W_1}{\left(W_0 - W_1/\rho\right)} \tag{4}$$

$$\varphi_s = \frac{d_p}{\left(d_p + P_c\right)} \tag{5}$$

$$D_s = \frac{D_o}{1 - \ln\left(\varphi_s\right)^2} \tag{6}$$

$$R = \frac{C_{\mathrm{DGT}}}{C_{\mathrm{Peeper}}} \tag{7}$$

$$K_d = \frac{C_s}{C_{\mathrm{Peeper}}} = \frac{H_1}{C_{\mathrm{Peeper}}} = \frac{1}{P_c} \cdot \frac{K_1}{K_{-1}} \tag{8}$$

$$T_c = \frac{1}{K_1 + K_{-1}} \tag{9}$$

$$K_1 = \frac{1}{T_c} \tag{10}$$

$$K_{-1} = \frac{K_1}{K_d \cdot P_c} \tag{11}$$

In this study, the acid-soluble/exchangeable fraction of Fe(II) [H_1 in Eq. (8)] was calculated following past reports [23]. Acetate buffer with a pH of 2.8 was used for extracting ferrous iron from the sediment [23].

2.5. Oxygen distribution at the SWB

The Planar Optrode (EasySensor instrument) COM6 device investigated the changes in oxygen content at the SWB in two-dimension (2D). The images measured using the PO device provided reliable information of the oxygen (hypoxia) distribution at the SWB in mm. The principle and usage of the Planar Optrode device can be found in past works [24].

2.6. Data analysis

Microsoft Excel 2016, Origin Software and SPSS 23 were used to process the data. The data was analysed using analysis of variance (ANOVA) in Origin 2018 Tool Pak. A significant value was set at 0.05. Each concentration obtained in the study represents the mean of at least three replicates.

3. Results and discussions

3.1. Variation in water temperature, DO, ORP and pH conditions from days 1 to 32

The 32-days field observation (November 22 to December 23) showing the water temperature, DO, ORP and pH conditions in Tianbao Reservoir with depth has been illustrated in Figs. 2, 3 and S1. The Tianbao Reservoir was greatly affected by the natural phenomenon of thermal stratification. At S3, the reservoir was thermally stratified from days 1 to 14

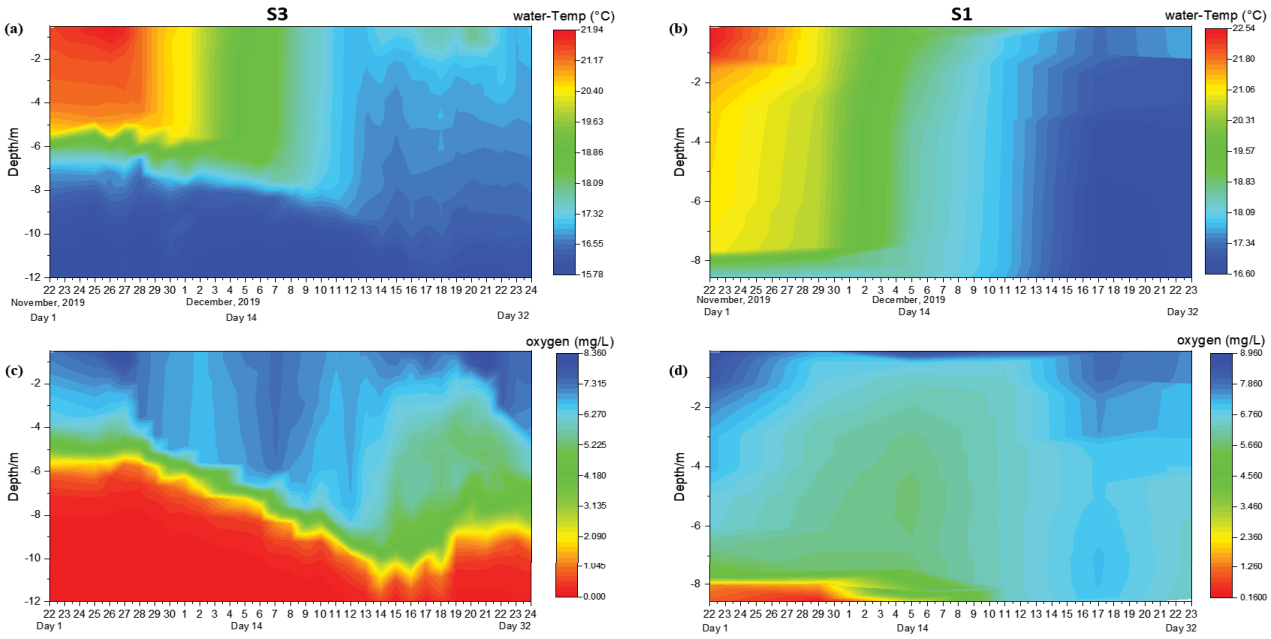

Fig. 2. Variation in (a, b) water temperature and (c, d) dissolved oxygen profiles at S3 and S1 of Tianbao Reservoir from November 22, 2019 (day 1) to December 23, 2019 (day 32). Data was collected at 12:00 each day. Water column depth = 12 m. Detailed temperature and dissolved oxygen variation at these sampling sites have been presented in Fig. S1.

with a significant difference ($p < 0.05$) in water temperature for the epilimnion (0–6 m) and hypolimnion (6–12 m) (Fig. 2a). The thermal stratification was weak after day 14 ($p > 0.05$) with an insignificant difference between the epilimnion and hypolimnion (Fig. 2c). The DO content was below 2 mg L^{-1} for the bottom water at S3, indicating the bottom water was hypoxic during the 35-days field observation. For S1, the thermal structure was weak and began to disappear around day 14 (Fig. 2b). The DO content in the bottom (benthic) water was hypoxic (smaller than 2 mg L^{-1}) for days 1 to 12 (December 3, 2019). However, the DO content was more than 5 mg L^{-1} after day 14 (Fig. 2d).

Fig. 3 gives an illustration of ORP and pH respectively at the sampling point S1. In this study, the ORP value increased when the DO concentration increased. Similarly, when the DO content decreased, the ORP also reduced, suggesting a reducing environment in the bottom water (Figs. 2 and 3). At S3, the ORP values at 11–12 m (bottom water) were negative throughout the 35-days field observation (Fig. 3a.). The ORP values (11–12 m) ranged from –199 to –95 mV while the pH varied from 6.8 to 7.2 at S3. Contrastingly, the ORP values at S1 were negative (at 8–8.5 m) from days 1 to 12 (December 3, 2019) and were positive (range: 121.8–290 mV) from days 14 to 32 due to the presence of oxygen. The pH during this period ranged from 6.8 to 7.2.

3.2. Variation in the concentration of total Fe, Mn, tannins, DOC, and sulfide in water samples of the reservoir from days 1 to 32

Table 2 shows the changes in the mean concentrations of total Fe (TFe), Mn, tannins, DOC and sulfide in the surface water and bottom water of the reservoir from days 1 to 35 at the sampling sites. The total Fe and Mn concentrations (S3) in the bottom water (6–12 m) were higher than that of the surface water (0–6 m) (Table 2) indicating the reservoir sediment serves as the source of Fe and Mn [25]. Specifically, for S3, the TFe in mg L^{-1} was from 0.04–0.17 in the surface water (epilimnion) while TFe in the bottom water (hypolimnion) was from 0.05–4.92 from days 1 to 35. For S1, the TFe measured in mg L^{-1} was from 0.04–0.77 in the surface water while TFe was from 0.05–4.92 mg L^{-1} in the bottom water from days 1 to 35. Similarly, Mn measured in mg L^{-1} was from 0.13–1.23 (S3) in the surface water while in the bottom water, Mn varied from 1.12 to 2.58 mg L^{-1} from days 1 to 35. For S1, the variation of Mn in the surface water ranged from 0.13 to 0.5 mg L^{-1} while it ranged from 0.5 to 2.8 mg L^{-1} in the bottom water. For S1, there was a slight decrease in the concentration of TFe in the epilimnion and hypolimnion from days 8 to 14 (Table 2). The variation of tannins over the 35-days field investigation showed an irregular sequence (Table 2). The range of tannins concentration (S3 and S1) in the surface water from days 1 to 35 was from 0.15 to 1.7 mg L^{-1} while that in the bottom water was from 0.14 to 2.84 mg L^{-1}. Specifically, there was a substantial depletion ($p < 0.05$) in the tannins content at S1 from days 1 to 8. Similarly, the substantial depletion ($p < 0.05$) in the tannins content at S3 occurred from days 8 to 14. The DOC concentration in the surface water ranged from 3.95% to 34.5% while the DOC concentration in bottom water ranged from 5.1% to 32.7%. Compared to the surface water, there was no significant change in DOC concentration at the bottom water. The sulfide concentration in the reservoir water was generally low throughout the field observation. The ranges of sulfide concentration were 0.005 to 0.011 mg L^{-1} and 0.005 to 0.012 mg L^{-1} for the surface and bottom water respectively (Table 2).

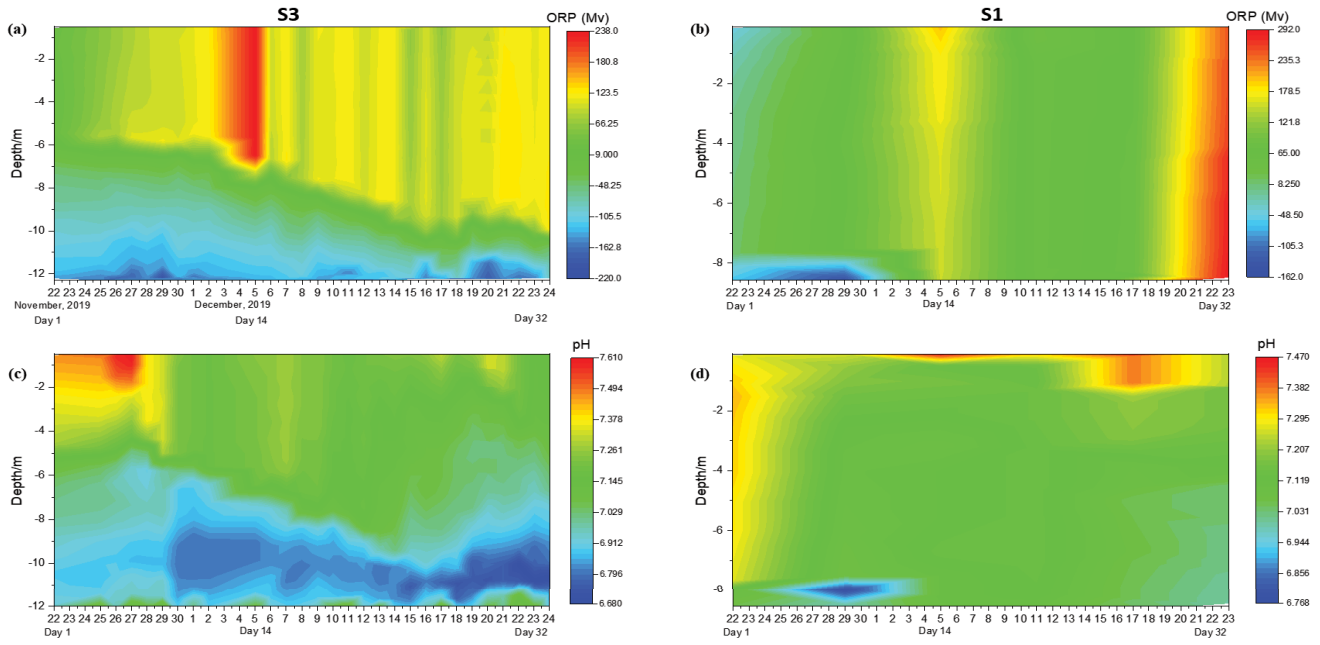

Fig. 3. Variation in (a, b) oxidation–reduction potential and (c, d) pH at S3 and S2 of Tianbao Reservoir with time from November 22, 2019 (day 1) to December 23, 2019 (day 32). Data was collected at 12:00 each day. Water column depth = 12 m. Detailed oxidation–reduction potential and pH variation at these sampling sites have been presented in Fig. S1.

Table 2
Concentration of total Fe, Mn, tannins, DOC and sulfide in water samples (surface and bottom water) of the reservoir

S3										
	Total Fe (mg L^{-1})		Total Mn (mg L^{-1})		Tannins (mg L^{-1})		DOC (mg L^{-1})		Sulfide (mg L^{-1})	
Days	Surface	Bottom	Surface	Bottom	Surface	Bottom	Surface	Bottom	Surface	Bottom
Day 1	0.04 ± 0.03^{a}	0.15 ± 0.01^{a}	0.13 ± 0.08^{a}	1.12 ± 1.13^{b}	1.35 ± 1.4^{a}	2.69 ± 0.04^{d}	23.1 ± 6.51^{a}	20.5 ± 1.84^{a}	0.005 ± 0.001^{a}	0.005 ± 0.001^{a}
Day 8	0.06 ± 0.06^{a}	1.92 ± 0.17^{b}	0.68 ± 0.67^{a}	2.39 ± 0.13^{c}	1.1 ± 0.07^{a}	2.84 ± 0.19^{d}	21.9 ± 1.56^{a}	17.0 ± 1.4^{a}	0.006 ± 0.001^{a}	0.007 ± 0.001^{a}
Day 14	0.13 ± 0.08^{a}	1.03 ± 0.02^{c}	1.23 ± 1.09^{b}	2.58 ± 0.11^{c}	0.18 ± 0.04^{bc}	0.41 ± 0.02^{c}	34.35 ± 2.48^{a}	27.3 ± 0.35^{a}	0.009 ± 0.001^{a}	0.008 ± 0.001^{a}
Day 21	0.04 ± 0.03^{a}	0.13 ± 0.01^{a}	0.56 ± 0.02^{a}	1.53 ± 0.04^{b}	0.17 ± 0.02^{bc}	0.21 ± 0.08^{c}	18.9 ± 12.45^{a}	24.1 ± 3.61^{a}	0.005 ± 0.001^{a}	0.008 ± 0.001^{a}
Day 32	0.04 ± 0.02^{a}	0.23 ± 0.23^{a}	0.55 ± 0.07^{a}	1.45 ± 0.07^{b}	0.16 ± 0.02^{bc}	0.23 ± 0.09^{c}	25.9 ± 0.99^{a}	27.3 ± 0.64^{a}	0.009 ± 0.001^{a}	0.009 ± 0.001^{a}
Day 35	0.17 ± 0.14^{a}	0.37 ± 0.25^{a}	0.71 ± 0.04^{a}	1.37 ± 0.66^{b}	0.28 ± 0.03^{bc}	0.38 ± 0.20^{c}	26.6 ± 3.29^{a}	23.3 ± 0.57^{a}	0.005 ± 0.001^{a}	0.005 ± 0.001^{a}
S1										
Day 1	0.4 ± 0.01^{a}	1.7 ± 0.04^{b}	0.13 ± 0.01^{a}	2.8 ± 0.04^{b}	1.7 ± 1.38^{a}	2.68 ± 0.17^{d}	26.4 ± 8.2^{a}	27.1 ± 0.21^{a}	0.005 ± 0.001^{a}	0.005 ± 0.001^{a}
Day 8	0.77 ± 0.85^{a}	0.98 ± 0.06^{a}	0.27 ± 0.01^{a}	0.98 ± 0.09^{c}	0.3 ± 0.04^{b}	0.5 ± 0.02^{b}	22.15 ± 5.16^{a}	21.6 ± 0.42^{a}	0.009 ± 0.001^{a}	0.001 ± 0.004^{a}
Day 14	0.21 ± 0.06^{a}	0.21 ± 0.01^{a}	0.5 ± 0.06^{a}	0.5 ± 0.05^{a}	0.16 ± 0.02^{b}	0.14 ± 0.01^{b}	28.9 ± 8.3^{a}	32.7 ± 0.57^{a}	0.009 ± 0.001^{a}	0.009 ± 0.001^{a}
Day 21	0.04 ± 0.01^{a}	0.11 ± 0.01^{a}	0.5 ± 0.01^{a}	0.64 ± 0.03^{a}	0.19 ± 0.0^{b}	0.23 ± 0.02^{b}	25.8 ± 3.5^{a}	27.9 ± 0.42^{a}	0.011 ± 0.002^{a}	0.012 ± 0.001^{a}
Day 32	0.05 ± 0.01^{a}	0.05 ± 0.01^{a}	0.5 ± 0.03^{a}	0.5 ± 0.02^{a}	0.15 ± 0.04^{b}	0.19 ± 0.02^{b}	28.7 ± 0.85^{a}	24.5 ± 0.35^{a}	0.010 ± 0.004^{a}	0.009 ± 0.001^{a}
Day 35	0.11 ± 0.02^{a}	0.15 ± 0.01^{a}	0.5 ± 0.01^{a}	0.48 ± 0.01^{a}	0.22 ± 0.02^{b}	0.25 ± 0.03^{b}	3.95 ± 1.16^{a}	5.1 ± 0.071^{a}	0.005 ± 0.001^{a}	0.005 ± 0.001^{a}

The concentration of TFe is sensitive to the variation in the ORP values. For S1, the ORP value was negative from days 1 to 12 and became positive from days 14 to 32 due to the presence of oxygen. This led to reduction of the concentration of TFe from 0.46 to 0.06 mg L^{-1} (i.e., from the negative period (days 1 to 12) to the positive period (days 14 to 32)). Similarly, the mean concentration of Mn reduced from 0.96 mg L^{-1} to 0.1 during this same period suggesting that Fe and Mn are controlled by the changes in the ORP values (Fig. 3 and Table 2).

Significantly different when the letters of each metal are different ($p < 0.05$, confidence interval 95%, descriptive statistics; $\alpha = 0.05$, one-way ANOVA.)

Each measured sample represents the mean of at least 5 replicates.

3.3. Spatial and temporal variation of Fe^{2+} Mn^{2+} and S^{2-} at the SWB on day 1

3.3.1. Pore water concentration and apparent flux of Fe^{2+} and Mn^{2+} on day 1

Fig. 4 is an illustration of the calculated pore water concentrations of Fe^{2+} and Mn^{2+} on day 1. The ranges (averages) of Mn^{2+} in mg L^{-1} at S1, S2, S3 and S4 were 5.23–9.76 (7.24), 5.84–8.98 (8.19), 0.22–10.72 (7.31) and 6.06–8.81 (7.89) respectively. That of Fe^{2+} were 7.43–18.37 (13.74), 14.99–30.11 (24.15), 6.34–16.99 (11.37) and 8.89–16.00 (11.82) respectively. The apparent fluxes of Mn^{2+} and Fe^{2+} at S1 to S4 are depicted in Fig. 4. For Mn^{2+} and Fe^{2+}, the differences in the apparent flux values at S1 to S4 were insignificant ($p < 0.05$). The fluxes for Fe^{2+} ranged from 34.5 to 141.37 mg m^{-2} d^{-1} while that of Mn^{2+} ranged from 3.95 to 12.3 mg m^{-2} d^{-1}. The maximum and minimum flux for Mn^{2+} happened at S4, and S1 respectively. Again, the maximum and minimum flux of Fe^{2+} happened at S2 and S4 respectively. The fluxes for Mn^{2+} and Fe^{2+} at S1 to S4 were positive.

3.3.2. Sulfide distribution and diffusive flux on day 1

The depth profile for S^{2-} at S1 to S4 on day 1 (November 22, 2019) is depicted in Fig. 4. The depth profile was calculated from the 2-D pictures depicted in Fig. S2. A varying distribution of S^{2-} was pictured at S1 to S4 (Fig. S2). The mean concentrations of S^{2-} (computed in mg L^{-1}) in the benthic water were 0.012, 0.016, 0.015, and 0.01 for S1, S2, S3 and S4 respectively. Similarly, the mean concentrations of S^{2-} (computed in mg L^{-1}) in the sediments were 0.023, 0.025, 0.024, and 0.031 for S1, S2, S3 and S4, respectively. The diffusive fluxes in mg m^{-2} d^{-1} of S^{2-} ranged from 0.0006 to 0.003, respectively (Fig. 4). The maximum and minimum flux occurred at S3 (0.003 mg m^{-2} d^{-1}) and S1 (6.02E-4 mg m^{-2} d^{-1}) respectively.

3.4. Variation in Fe^{2+} and DOC (Eucalyptus sp. leaves) in reservoir sediments from days 1 to 32

The spatial variations in the depth profile of DGT labile Fe and DOC for days 1, 14 and 32 have been depicted in Fig. 5. The content of DGT-labile Fe during the field study showed a low mean concentration (<1 mg L^{-1}) in the overlying (benthic) water and a high concentration (>10 mg L^{-1}) within the sediments for S3 and S1 (Fig. 5). The changes in the vertical profile of DGT-labile Fe increased with depth (from 30 to –30 mm) and later remained constant with depth (from –30 to –110 mm). The average concentrations of DGT-labile Fe for S3 in the overlying (benthic) water were 0.78, 0.93 and 0.09 mg L^{-1} for days 1, 14 and 32, respectively. At S1, the average concentrations of DGT-labile Fe (computed in mg L^{-1}) in the overlying (benthic) water were 0.95, 0.73 and 0.18, respectively (Fig. 8). There was a significant decrease in Fe^{2+} concentration in the overlying water for S3 and S1 from days 1 to 32 indicating that Fe^{2+} was consumed during the 32-days field observation (Figs. 5 and 6). For the concentration of DGT-labile Fe in the sediments, the mean concentration for S3 on days 1, 14 and 32 were 12.52, 11.13 and 11.81 mg L^{-1} respectively. Similarly, concentrations at S1 were 14.71, 16.59, and 15.87 mg L^{-1} respectively. There was no significant difference in Fe^{2+} concentration in the sediment for S3 and S1 from days 1 to 32 (Fig. 6). A high positive apparent flux for Fe^{2+} was observed from days 1 to 32 (Fig. 7). The flux (Fe^{2+}) increased from days 1 to 14 and decreased significantly ($p < 0.05$) after day 14 for both S3 and S1.

For DOC, the mean concentration in the overlying (benthic) water was significantly ($p < 0.05$) lower than that in sediments (Fig. 6). At S3 and S1, the mean concentration recorded in the overlying water over the 32-days period fell below 12% while the mean concentration of DOC in the sediments was more than 22% (Fig. 6). The changes in the vertical profile of DOC were similar to that of Fe^{2+}. DOC concentration increased with depth (from 30 to –20 mm) and later remained constant with depth (from –20 to –110 mm). Specifically, the mean concentrations of DOC in the overlying water for S3 were 11.84%, 3.87%, 5.02% for days 1, 14 and 32 respectively while that of S1 was 11.35%, 9.2%, 5.53% for days 1, 14 and 32, respectively. There was a significant decrease in DOC concentration in the overlying water for S3 and S1, indicating that DOC was also consumed during the 32-days field observation as recorded for Fe^{2+} (Fig. 6). As indicated in Fig. 6, there was a significant change ($p < 0.05$) for the DOC concentration in the overlying water for day 14 compared to day 1. The trend was similar ($p < 0.05$) when the DOC concentration for day 32 was compared to day 1 for both S3 and S1 in the overlying (benthic) water. For S3, the content of DOC in the sediments on days 1, 14 and 32 were 30.37%, 22.55%, 29.16% respectively while that of S1 were 34.61%, 26.79%, 36.03%, respectively. There was no significant difference in DOC concentration in the sediment for S3 and S1 when day 1 was compared to that of day 32. However, the difference was significant ($p < 0.05$) in the overlying water (for S3 and S1) when day 1 was compared to day 14 (Fig. 6). During this period, the variation in oxygen molecules at the SWB was monitored (Fig. 7). For S3, the SWB was hypoxic during the 32-day field observation while oxygen was detected on days 14 and 32 for S1.

3.5. Variation in the remobilization/replenishment of Fe^{2+} from days 1 to 32

DIFS model parameters for days 1, 14 and 32 are presented in Table 5. After running the model, K_{-1}, K_1 and T_c,

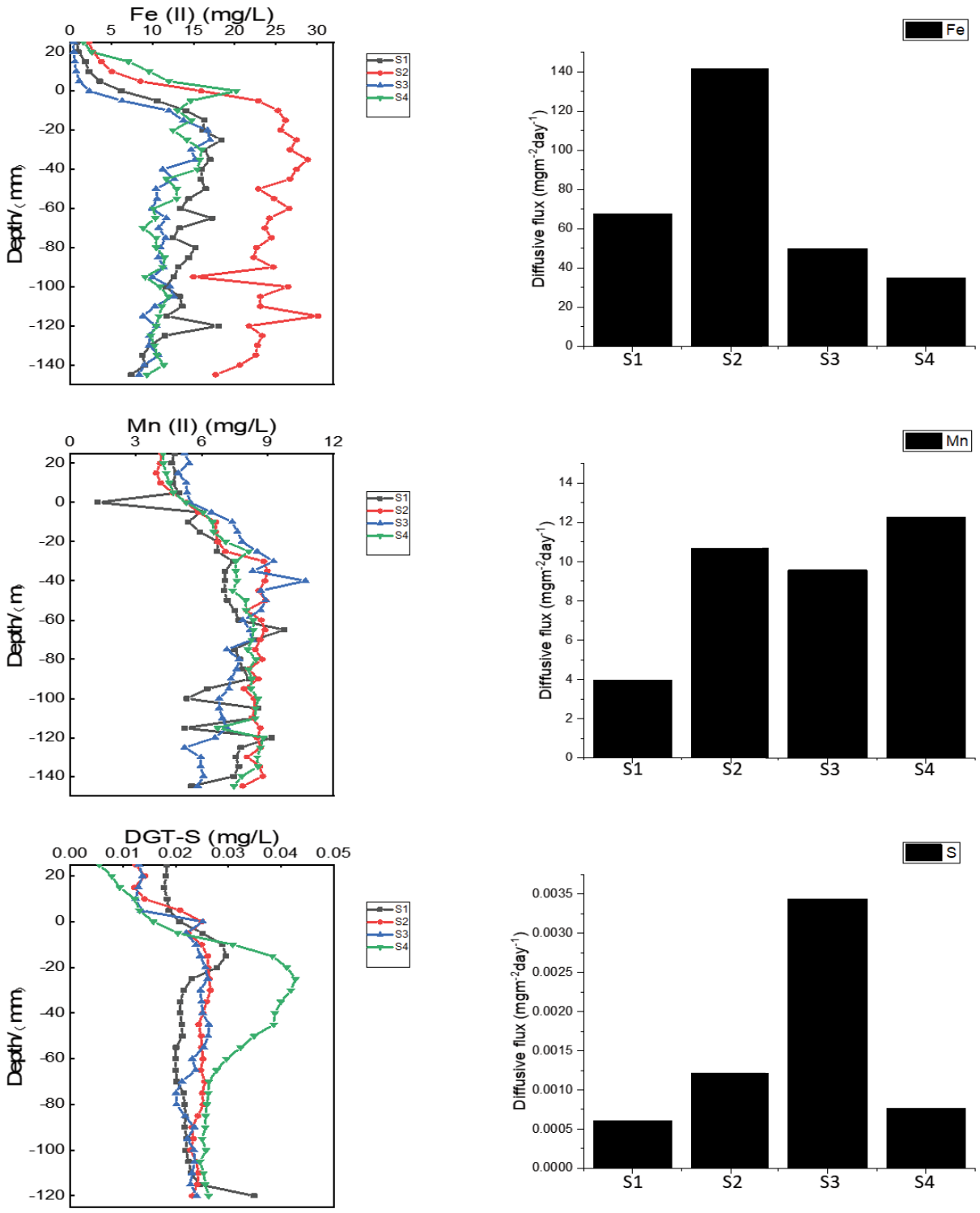

Fig. 4. Distributions of pore water concentrations and apparent flux of Fe^{2+}, Mn^{2+} and S^{2-} with depth at the sampling sites (S1–S4) in Tianbao Reservoir on day 1.

were measured (Table 5). Fig. 8 consists of graphical representations of changes in resupply parameter (R) values against the deployment time (T) for Fe^{2+} in Tianbao Reservoir. For S3, the resupply parameter (R) value recorded during the hypoxic period was greater than 0.7 for both days 1 and 14 and later decreased to 0.44 on day 32. For S1, the R-value for days 1, 14, 32 were 0.72, 0.46 and 0.68, respectively.

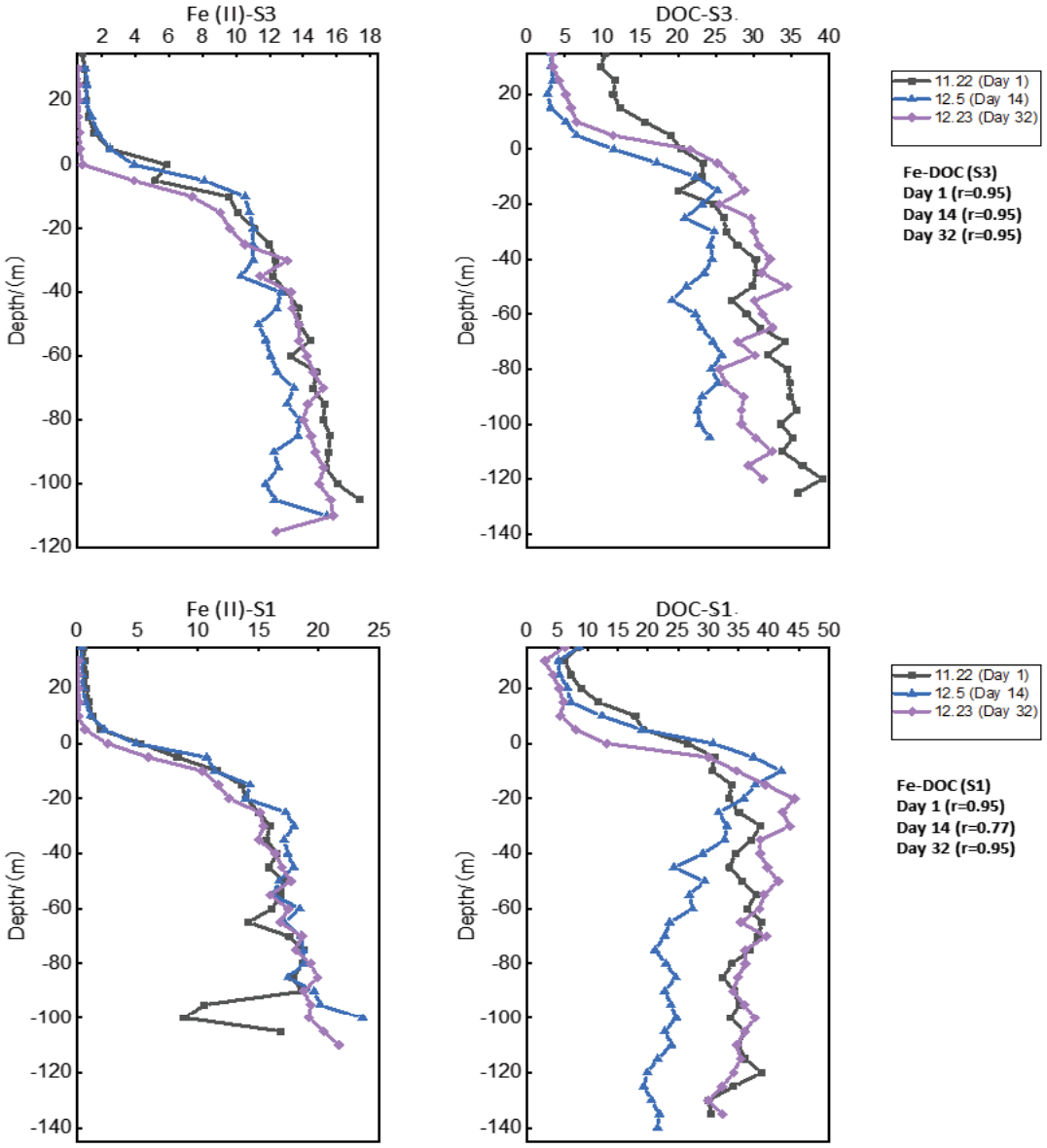

Fig. 5. Temporal and vertical profile variations of the concentrations Fe^{2+} and DOC at S3 and S1 during the 32-days field investigation.

4. Discussion

4.1. Role of metal fluxes and tannins from Eucalyptus sp. leaves in water blackening

4.1.1. Variation of Fe^{2+}, Mn^{2+}, S^{2-} fluxes due to redox conditions

Diffusive flux (Fick's first law) obtained from the DGT device between the sediment and water provides reliable information on the dynamics of pollutants at the SWB compared to traditional ex-situ methods [26]. For Fe^{2+} and Mn^{2+}, the positive net diffusive flux (range: 34.5 to 141.37 and 3.95 to 12.3 mg m^{-2} d^{-1} respectively) proved that Fe^{2+} and Mn^{2+} moved from the sediment to the hypoxic overlying water. The mean diffusive flux of Fe^{2+} (73.25 mg m^{-2} d^{-1}) identified in the present research was substantially greater than that of other reservoirs in China like Aha Reservoir (5.58 mg m^{-2} d^{-1}) and Hongfeng Reservoir (0.89 mg m^{-2} d^{-1}). Likewise, the mean flux of Mn^{2+} (9.11 mg m^{-2} d^{-1}) was greater than that of China's Jinpen Reservoir (7.5 mg m^{-2} d^{-1}). The study found an average flux of 0.002 mg m^{-2} d^{-1} for S^{2-} in contrast with the negative mean flux observed in Taihu Lake, China.

The incidence of black water events in water bodies has been attributed to hypoxic environments and the availability of divalent/trivalent metals [17]. From our study, the limited DO content at the SWB (pictured in Figs. 2 and 7) was primarily attributable to reservoir thermal stratification, which created a reducing environment in the process. In a hypoxic setting, the biogeochemical cycle of Fe, Mn and S is greatly affected by sulphate-reducing bacteria (SB) and iron-reducing bacteria (IB). Hypoxia and negative ORP

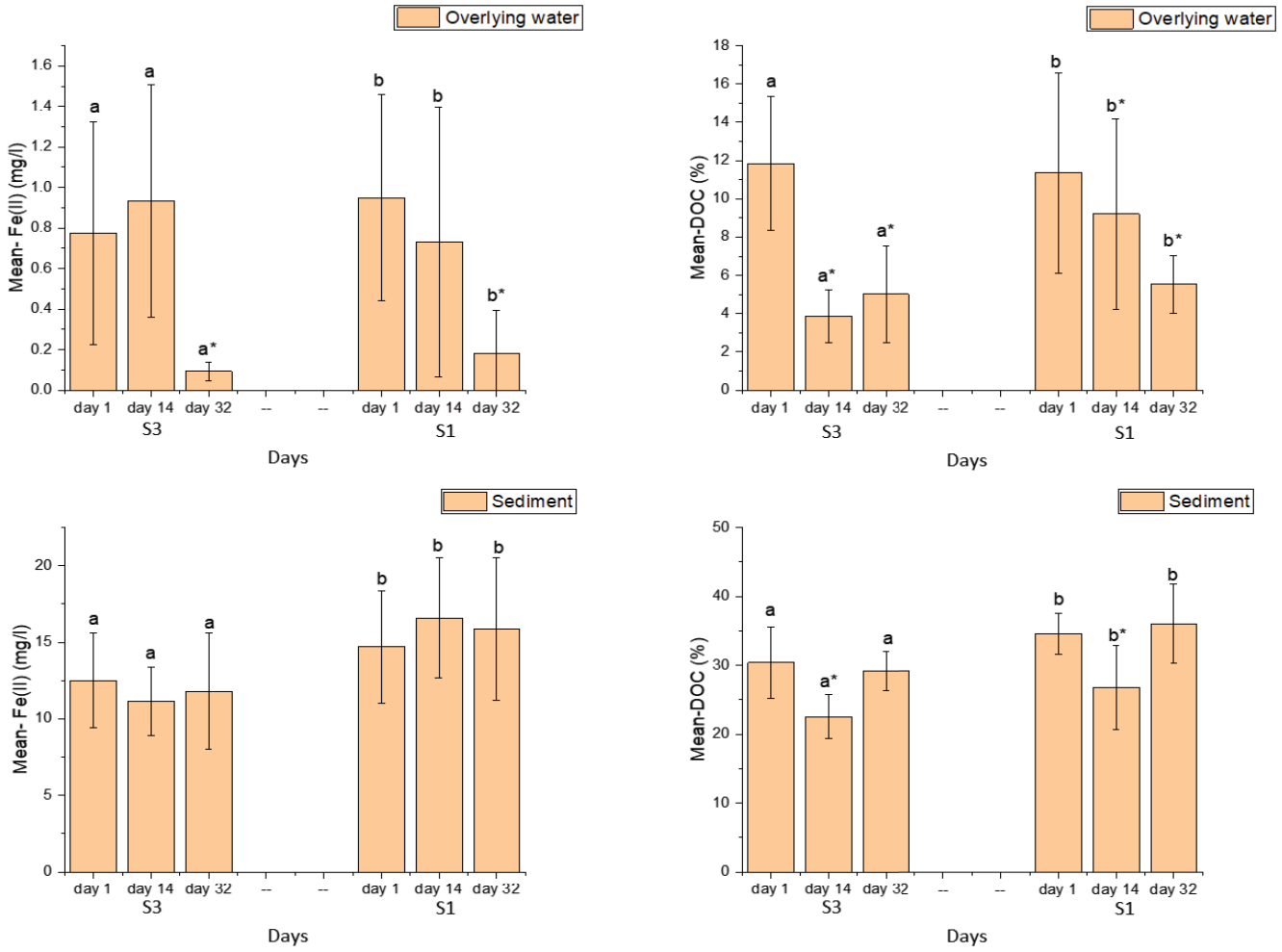

Fig. 6. Variation in Fe(II) and DOC mean concentration in the overlying water and sediment at S3 and S1 during the 32-days field investigation. a*/b*: significantly different when Fe(II) and DOC concentration on days 14 and 32 is compared to that of day 1 ($p < 0.05$, confidence interval 95%, descriptive statistics; $\alpha = 0.05$, one-way ANOVA.

provides the optimal environment for the efficient functioning of SBs and IBs. SBs and IBs convert iron, manganese and sulfide into their divalent and trivalent forms combining to generate black precipitates (FeS and MnS). The positive relationship observed (Table 3, Figs. S3 and S4) for iron–sulphur ($r > 0.06$, $p < 0.05$) and manganese-sulfur ($r > 0.25$, $p < 0.05$) confirmed that the source of the black sediments in the reservoir was due to Fe and Mn.

4.1.2. Fe^{2+} and *Eucalyptus* sp. leaves (tannins) interaction

Reducing conditions (low oxygen and low ORP) cause significant metal efflux to the overlying (benthic) water from the sediments. On the other hand, the efflux of metals is low when the conditions are oxidizing [5]. In this study, the fluxes of Fe^{2+} were variable during the 35-days field investigation due to the different reducing conditions. Based on the diffusive fluxes measured, the oscillations were low during the oxidizing conditions and were high during the reducing environment (S1, Fig. 6). This variation of the fluxes corresponded with changes in DO concentration and ORP values at the overlying water of the reservoir. For S3, the low ORP values and DO concentration observed during the 35-days observation period indicated that the primary electron-accepting mechanism responsible for the high Fe^{2+} at the SWB was Fe reduction [27]. For S1, day 1 had a highly reduced environment compared to days 14 and 32 (Fig. 3). The results revealed that the Fe-reduction process was already taking place on day 1. The Fe^{2+} flux decreased when the environment changed from a reducing condition (day 1) to the oxidizing environment (day 14). The Fe^{2+} flux reduction was even significant ($p < 0.05$) when the reducing conditions completely disappeared on day 32 (Fig. 6).

The tannins from *Eucalyptus* sp. trees are substantially greater than that of other aquatic plants. Water bodies that contain *Eucalyptus* sp. leaves change colour due to the existence of tannins [3]. In this study, *Eucalyptus* sp. trees which mainly surround the Tianbao Reservoir affected the reservoir water quality by altering the tannins concentration in the reservoir. The mean and range of the tannin's concentration recorded in the reservoir was 1.94 and 0.2–2.7 mg L^{-1} respectively (Table 2). The 32-days field

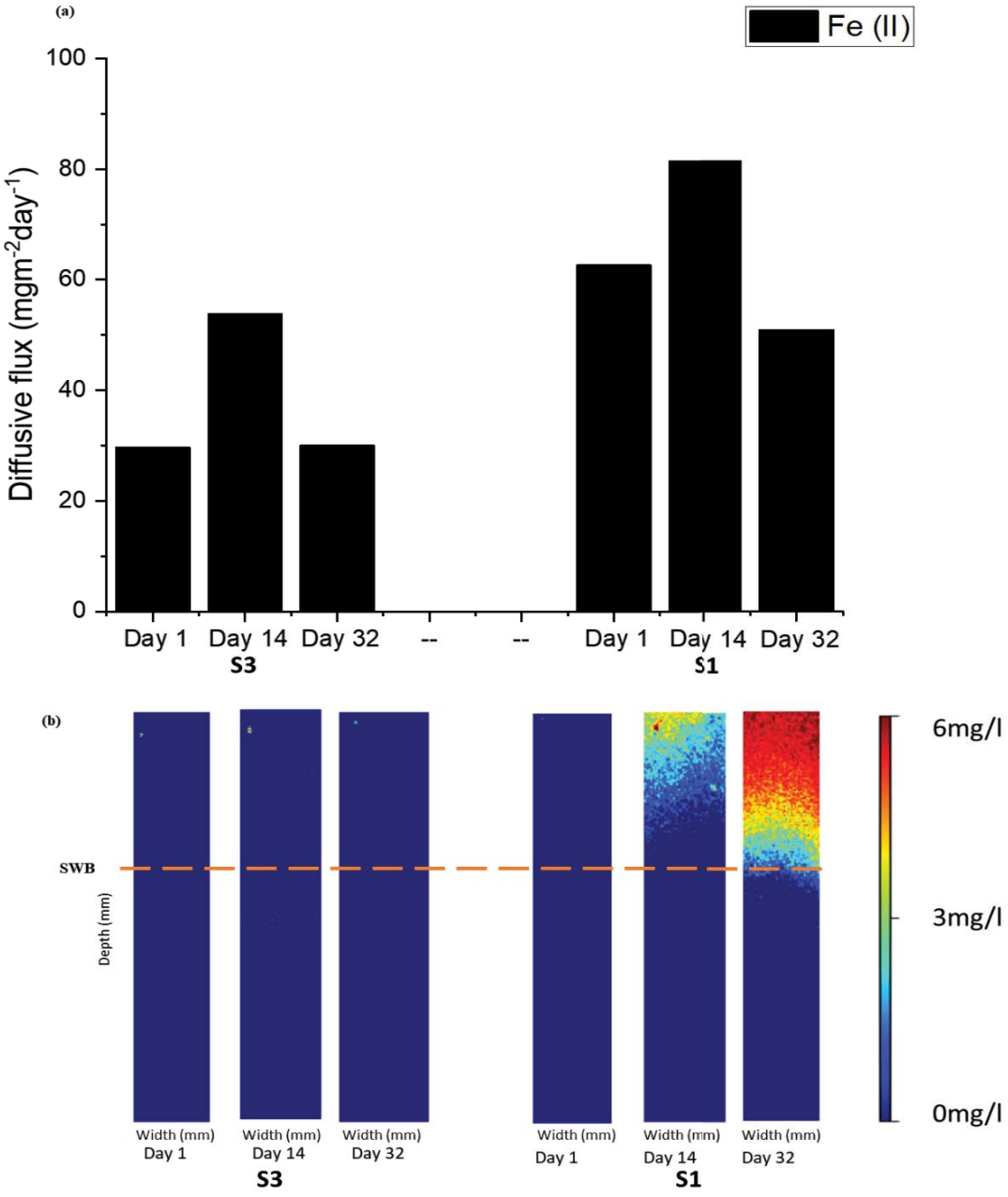

Fig. 7. The 32-days field investigation at S3 (depth = 12 m) and S1 (depth = 8.5 m) showing (a): apparent flux of Fe^{2+} (II) and (b): the variation in oxygen concentration at the sediment water boundary (SWB).

Table 3
Correlation analysis (r^2) for Fe^{2+}, Mn^{2+} and S^{2-} at the sampling sites

r^2	S1	S2	S3	S4
Fe–S	0.3	0.8	0.6	0.3
Mn–S	0.1	0.6	0.5	0.4

investigation conducted on the reservoir suggested that the thermal structure in the reservoir began to disappear on day 14 causing the mixing of the reservoir water column (allowing the Fe^{2+} ions to move freely from the bottom water to surface water). Similarly, the reservoir water blackening occurred on day 14 suggesting that both the black precipitates (FeS and MnS) and Fe^{2+} were transported from the overlying water throughout the water column when the thermal structure ceased to exist. The later (Fe^{2+}) then reacted with *Eucalyptus* sp. trees' tannins to form black substance (Fig. S5) [3]. This assertion was further supported by the substantial decrease ($p < 0.05$) in the concentration of tannins in the reservoir between days 8 and 14 (Table 2). Subsequently, the substantial decrease ($p < 0.05$) in Fe^{2+} ions content from day 1 (no black water) today 32 (black water) also suggested that Fe^{2+} was consumed during the complexation reaction with *Eucalyptus* sp. tannins. The

high correlation between Fe-DOC (Table 4) further indicated that black materials formed in the reservoir were due to the complexation reaction between Fe^{2+} and DOC.

4.2. Replenishment ability/remobilization behaviour of Fe^{2+}

Numerous studies have used the DGT-DIFS model to analyse the kinetics, release dynamics and the remobilization of elements at the SWB [4]. The DGT-DIFS program provides a better understanding of the remobilization of Fe^{2+} at the SWB under different reducing (ORP) conditions. The resupply parameter (R) from our study provided important details on Fe reactivity and susceptibility within the sediments [28]. After simulation of the model, the parameters (T_c, K_1 and K_{-1}) (Table 5) were used to assess the kinetic characteristics and release mechanism of Fe^{2+} in the sediment at the micro-level [28]. The R-values describe the level of reactivity of Fe within the sediments. R-value of 1 means sediment is profoundly reactive whiles R-value of 0 means sediment is not reactive [14]. The R-value for S3 was reactive (0.75) on day one but a decrease in the level of reactivity on days 14 and 32 was recorded with R-values of 0.71 and 0.44, respectively. For S1, a similar trend was observed with the reactivity decreasing from 0.72 (day 1) to 0.46 (day 14). The decrease in the reactivity of Fe^{2+} from days 1 to 32 may be due to the change in the reducing environment and production of black precipitate (FeS and MnS as discussed in section 4.2.1) in the sediments on day 14 (reservoir colour begins to change to black on day 14). These black materials produced may be the cause of the reduction in the reactivity of Fe^{2+} in the sediments. The decrease in reactivity also indicates that that the sediments (day 1) at S3 and S1 could quickly liberate Fe^{2+} to the benthic water than on days 14 and 32 [29]. In fact, on day 32, the lowest extent partially sustained case was computed at S3 with a R-value of 0.44. The lowest reactivity occurring at S3 (day 32) was further supported by the lowest average mean value of Fe^{2+}concentration recorded in the overlying water. Demonstrating that the sediments could not release Fe^{2+} to the overlying water on day 32 compared to day 1. The mean Fe^{2+} concentration in day 1 was significantly higher ($p < 0.05$) than that for day 32 in the overlying water.

Numerous studies have revealed SBs and IBs co-exist in a hypoxic environment [17] and are responsible for the production Fe^{2+} and S^{2-} in the overlying water. In this study, S3 was hypoxic throughout the 32-days with an increased production of FeS. The reactivity of Fe^{2+} thus decreased in the sediment in this order: day 1 (R = 0.75) > day 14 (R = 0.71) > day 32 (R = 0.44). For S1, hypoxia existed from days 1 to 12; however, the DO content was greater than 5 mg L^{-1} after day 14. The higher DO content revealed that the production of FeS in the SWB at S1 ceased since SBs and IBs responsible for Fe^{2+} and S^{2-} production function in a hypoxic environment [30,31]. This may explain the insignificant and irregular pattern for the sediments reactivity after day 14 (S1).

According to the different R-values chart (Fig. 8), the resupply mechanism of Fe^{2+} in the sediments from days 1 to 32 (under different reducing conditions) can be grouped as the non-steady-state case. This falls under the "partially sustained" category [28]. The maximum desorption rate (K_{-1}) for S3 and S1 occurred on day 1 and reduced following this sequence: day 1 > day 14 > day 32 as presented in

Table 4
Correlation analysis (r^2) for Fe^{2+} and DOC at the sampling sites during the 32-days field investigation

Sampling sites	r^2	Day 1	Day 14	Day 32
S3	Fe-DOC	0.9	0.9	0.9
S1	Fe-DOC	0.9	0.6	0.9

Table 5
The input and output parameters of the DIFS model

Input											
Time	Site	R	K_d ($cm^3\ g^{-1}$)	P_c ($g\ cm^{-3}$)	D_o ($cm^2\ s^{-1}$)	D_S ($cm^2\ s^{-1}$)	ϕ_d	ϕ_s	C_o ($mg\ L^{-1}$)	F_1 ($mg\ g^{-1}$)	C_{DGT} ($mg\ L^{-1}$)	Δg (cm)
Day 1	S3	0.75	62.92	0.42	5.57E-06	4.31E-06	0.75	0.86	9.17	0.58	6.87	0.093
Day 1	S1	0.72	48.77	0.58	5.57E-06	3.99E-06	0.75	0.82	13.86	0.68	9.94	0.093
Day 14	S3	0.71	141.55	0.28	5.57E-06	4.648E-06	0.75	0.91	12.33	1.75	8.82	0.093
Day 14	S1	0.46	83.00	0.24	5.57E-06	4.74E-06	0.75	0.92	24.07	1.99	11.04	0.093
Day 32	S3	0.44	83.92	0.58	5.57E-06	3.99E-06	0.75	0.82	11.77	0.98	5.13	0.093
Day 32	S1	0.68	71.58	0.87	5.57E-06	3.55E-06	0.75	0.75	9.71	0.69	6.60	0.093

Output				
Time	Site	T_c (d)	K_1 (d^{-1})	K_{-1} (d^{-1})
Day 1	S3	0.21	4.68	0.18
Day 1	S1	0.25	4.04	0.14
Day 14	S3	0.29	3.42	0.09
Day 14	S1	1.62	0.62	0.03
Day 32	S3	0.29	3.46	0.07
Day 32	S1	1.57	0.64	0.01

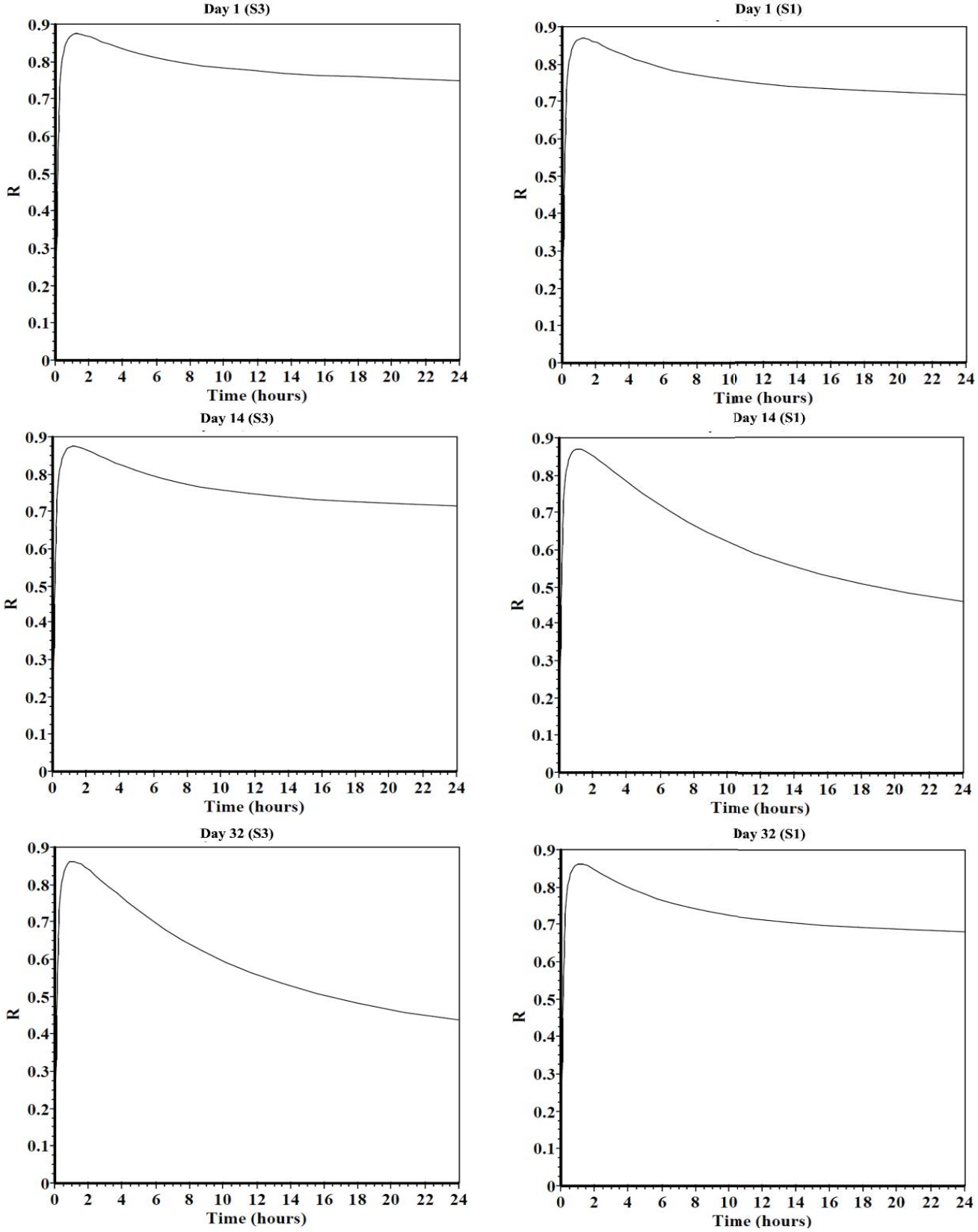

Fig. 8. Time dependency of *R* curves for Fe(II) during the 32-days field investigation at S3 (depth = 14 m) and S1 (depth = 10 m) obtained from the DIFS model.

Table 5. The T_c parameter gives details about the (de)sorption response time, with S3 recording the highest time (0.29 d) on day 32, which coincided with the lowest K_{-1} value of 0.07 d^{-1}. This indicated that the resupply kinetics of Fe^{2+} ions from the sediment to the pore (benthic) water was the slowest on day 32. Similarly, on day 1, S3 recorded the lowest response time for (de)sorption of 0.21 d (corresponding to the highest K_{-1} (0.18 d^{-1}). The exchange dynamics of Fe^{2+} ions between the pore (benthic) water and sediment was highest and occurred on day 1.

4.3. Implications of black water on aquatic ecosystem and management practices

Several studies [4,17] have proclaimed that black water development (associated with high tannins concentration from *Eucalyptus* plantation and FeS production from the hypoxic SWB) impedes the movement of sunlight into the water system which affects the photosynthesis of plants and algae and in turn disturbs the aquatic environment cycle. The results from our study support these arguments in that it reveals how the occurrence of the reservoirs blackening takes place. Furthermore, the study demonstrated how tannins from *Eucalyptus* plantation and trace metals from the reservoir sediments contribute to water quality deterioration of reservoirs. The physical habitat of the aquatic environment will be affected negatively due to low light penetrations. This will affect fish productivity as well as insecurity among water consumers [17]. The water systems (reservoirs) must be guarded from the development of BW events. The main source of tannins responsible for the occurrence of BW events is the leaves from the *Eucalyptus* plantation. The continuous logging of *Eucalyptus* trees on a large scale around the reservoirs will be catastrophic to the aquatic habitat since these leaves will find their way into the reservoir via wind or precipitation. To curb this problem, which does not only affect water quality but also poses as a risk to the health of water systems, careful monitoring and regulations of *Eucalyptus* trees should be implemented. Logging should not be done during the rainy season since heavy rains drive the fresh *Eucalyptus* leaves into the water systems. Also, the new leaves should be dried after logging to reduce the tannins content in the leaves (in case the leaves find its way into the water system). Secondly, the building of buffer zones to stop fresh leaves from the *Eucalyptus* plantation from moving into the reservoir may also be needed. Thirdly, the *Eucalyptus* trees can be planted alongside other trees with fewer tannins concentration to reduce its impact on water systems. The formation of black materials (FeS and MnS) due to trace metals in reservoir sediments is greatly enhanced by hypoxia. Fourthly, the use of air aeration system to pump oxygen at SWB will effectively reduce the production FeS and MnS [32]. Finally, the erection of wells at a different spacing in the reservoir will efficiently inject chemical oxidants into the reservoir sediments to prevent the production of FeS and MnS [31].

5. Conclusion

In this study, we used the DGT, HR-peeper, planar optode, DGT-DIFS model to determine the cause of BW events. The 35-days experiment showed conclusively that the content of Fe^{2+} and Mn^{2+} ions were high in reservoir sediments. The results indicated that the presence of hypoxia was crucial to the substantial fluxes (Fe^{2+}, Mn^{2+}, S^{2-}) detected at the SWB. The co-precipitation of Fe^{2+}, Mn^{2+}, S^{2-} generated black substances (manganese and iron sulfides) at the benthic region (SWB). A substantial decrease ($p < 0.05$) in Fe^{2+}, DOC and tannins (tannic acid) content from days 1 to 32 indicated that the reaction between Fe^{2+}, DOC and tannins (tannic acid) also caused BW.

The DGT-DIFS program showed that the resupply mechanism of Fe^{2+} ions in the sediments (S3 and S1) from days 1 to 32 can be grouped as "non-steady-state case". Belonging to the "partially sustained" category under different reducing conditions. The findings from the field investigation present useful information for the planning, design, and protection of water systems from deterioration.

Compliance with ethical standards

Conflict of interest

The authors declare that they have no conflict of interest.

Acknowledgments

The research was supported by the National Key Research and Development Program of China (2017YFC0405203, 2016YFC0401703) and the Chinese National Science Foundation (51779072, 51809102). Further support came from the Major Science and Technology Program for Water Pollution Control and Treatment (2017ZX07204003) and Fundamental Research Funds for the Central Universities (B200204014).

References

[1] Q. Chen, J. Chen, J. Wang, J. Guo, Z. Jin, P. Yu, Z. Ma, In situ, high-resolution evidence of phosphorus release from sediments controlled by the reductive dissolution of iron-bound phosphorus in a deep reservoir, southwestern China, Sci. Total Environ., 666 (2019) 39–45.

[2] K.M. Krueger, C.E. Vavrus, M.E. Lofton, R.P. McClure, P. Gantzer, C.C. Carey, M.E. Schreiber, Iron and manganese fluxes across the sediment-water interface in a drinking water reservoir, Water Res., 182 (2020) 116003, doi: 10.1016/j.watres.2020.116003.

[3] F. Luo, Y. Li, E. Norgbey, R. Li, Z. Ya, A.S. Nwankwegu, H. Lie, L. Sarpong, A study on the occurrence of black water in reservoirs in *Eucalyptus* Plantation region, Environ. Sci. Pollut. Res., 27 (2020) 34927–34940.

[4] E. Norgbey, Y. Li, Z. Ya, R. Li, A.S. Nwankwegu, G.E. Takyi-Annan, F. Luo, W. Jin, Y. Huang, L. Sarpong, High resolution evidence of iron-phosphorus-sulfur mobility at hypoxic sediment water interface: an insight to phosphorus remobilization using DGT-induced fluxes in sediments model, Sci. Total Environ., 724 (2020) 138204, doi: 10.1016/j.scitotenv.2020.138204.

[5] K.M. Krueger, C.E. Vavrus, M.E. Lofton, R.P. McClure, P. Gantzer, C.C. Carey, M.E. Schreiber, Iron and manganese fluxes across the sediment-water interface in a drinking water reservoir, Water Res., 182 (2020) 116003, doi: 10.1016/j.watres.2020.116003.

[6] N. Rong, W. Lu, C. Zhang, Y. Wang, J. Zhu, W. Zhang, P. Lei, In situ high-resolution measurement of phosphorus, iron and sulfur by diffusive gradients in thin films in sediments of black-odorous rivers in the Pearl River Delta region,

South China, Environ. Res., 189 (2020) 109918, doi: 10.1016/j.envres.2020.109918.
[7] M. Calviño-Cancela, E.J.B. van Etten, Invasive potential of *Eucalyptus globulus* and *Pinus radiata* into native eucalypt forests in Western Australia, For. Ecol. Manage., 424 (2018) 246–258.
[8] A.C. Ferraz Filho, J.R.S. Scolforo, B. Mola-Yudego, The coppice-with-standards silvicultural system as applied to *Eucalyptus* plantations — a review, J. For. Res., 25 (2014) 237–248.
[9] B. Engler, G. Becker, S. Hoffmann, Process mechanization models for improved *Eucalyptus* plantation management in Southern China based on the analysis of currently applied semi-mechanized harvesting operations, Biomass Bioenergy, 87 (2016) 96–106.
[10] G. Yang, M. Wen, Y. Deng, X. Su, D. Jiang, G. Wang, Y. Chen, G. Chen, S. Yu, Occurrence patterns of black water and its impact on fish in cutover areas of *Eucalyptus* plantations, Sci. Total Environ., 693 (2019) 133393, doi: 10.1016/j.scitotenv.2019.07.199.
[11] X. Yang, D. Li, K. McGrouther, W. Long, Y. Li, Y. Chen, X. Lv, N.K. Niazi, Z. Song, H. Wang, Effect of *Eucalyptus* forests on understory vegetation and soil quality, J. Soils Sediments, 17 (2017) 2383–2389.
[12] J. Cao, Q. Sun, D. Zhao, M. Xu, Q. Shen, D. Wang, Y. Wang, S. Ding, A critical review of the appearance of black-odorous waterbodies in China and treatment methods, J. Hazard. Mater., 382 (2019) 121511, doi: 10.1016/j.jhazmat.2019.121511.
[13] S. Ding, Q. Sun, D. Xu, F. Jia, X. He, C. Zhang, High-resolution simultaneous measurements of dissolved reactive phosphorus and dissolved sulfide: the first observation of their simultaneous release in sediments, Environ. Sci. Technol., 46 (2012) 8297–8304.
[14] M.P. Harper, W. Davison, H. Zhang, W. Tych, Kinetics of metal exchange between solids and solutions in sediments and soils interpreted from DGT measured fluxes, Geochim. Cosmochim. Acta, 62 (1998) 2757–2770.
[15] R. Li, Z. Wu, L. Li, D. Cai, L. Huang, J. Tao, F. Luo, E. Norgbey, Simulation of fish migration at different water depths based on backpropagation neural network, Appl. Ecol. Environ. Res., 17 (2019) 437–449.
[16] I. Bisutti, I. Hilke, M. Raessler, Determination of total organic carbon – an overview of current methods, TrAC, Trends Anal. Chem., 23 (2004) 716–726.
[17] N. Rong, W. Lu, C. Zhang, Y. Wang, J. Zhu, W. Zhang, P. Lei, In situ high-resolution measurement of phosphorus, iron and sulfur by diffusive gradients in thin films in sediments of black-odorous rivers in the Pearl River Delta region, South China, Environ. Res., 189 (2020) 109918, doi: 10.1016/j.envres.2020.109918.
[18] K.J. Marsh, C. Kulheim, S.P. Blomberg, A.H. Thornhill, J.T. Miller, I.R. Wallis, D. Nicolle, J.-P. Salminen, W.J. Foley, Genus-wide variation in foliar polyphenolics in eucalypts, Phytochemistry, 144 (2017) 197–207.
[19] Z. Wu, S. Wang, L. Zhang, L. Jiao, DGT induced fluxes in sediments model for the simulation of phosphorus process and the assessment of phosphorus release risk, Environ. Sci. Pollut. Res., 23 (2016) 14608–14620.
[20] H. Tamura, K. Goto, T. Yotsuyanagi, M. Nagayama, Spectrophotometric determination of iron(II) with 1,10-phenanthroline in the presence of large amounts of iron(III), Talanta, 21 (1974) 314–318.
[21] J. Soto-Neira, Q. Zhu, R.C. Aller, A new spectrophotometric method to quantify dissolved manganese in marine pore waters, Mar. Chem., 127 (2011) 56–63.
[22] L.G. Murray, S.M. Mudge, A. Newton, J.D. Icely, The effect of benthic sediments on dissolved nutrient concentrations and fluxes, Biogeochemistry, 81 (2006) 159–178.
[23] K. Kumada, T. Asami, A new method for determining ferrous iron in paddy soils, Soil Sci. Plant Nutr., 3 (1957) 187–193.
[24] S. Li, Ding, L. Yang, Q. Zhu, M. Chen, D.C.W. Tsang, G. Cai, C. Feng, Y. Wang, C. Zhang, Planar optode: a two-dimensional imaging technique for studying spatial-temporal dynamics of solutes in sediment and soil, Earth-Sci. Rev., 197 (2019) 102916, doi: 10.1016/j.earscirev.2019.102916.
[25] C. Han, S. Ding, L. Yao, Q. Shen, C. Zhu, Y. Wang, D. Xu, Dynamics of phosphorus-iron-sulfur at the sediment-water interface influenced by algae blooms decomposition, J. Hazard. Mater., 300 (2015) 329–337.
[26] Li, T. Huang, X. Mao, H. Zhang, K. Li, G. Wen, X. Lv, L. Deng, Controlling reduced iron and manganese in a drinking water reservoir by hypolimnetic aeration and artificial destratification, Sci. Total Environ., 685 (2019) 497–507.
[27] W.W. Ma, M.X. Zhu, G.P. Yang, T. Li, In situ, high-resolution DGT measurements of dissolved sulfide, iron and phosphorus in sediments of the East China Sea: insights into phosphorus mobilization and microbial iron reduction, Mar. Pollut. Bull., 124 (2017) 400–410.
[28] W. Yan, L. Liu, T. Wu, L. Song, H. Wang, Z. Lu, B. Li, Y. Zhu, Effects of short-term aerobic conditions on phosphorus mobility in sediments, J. Freshwater Ecol., 34 (2019) 649–661.
[29] Z. Wu, S. Wang, N. Ji, Phosphorus (P) release risk in lake sediment evaluated by DIFS model and sediment properties: a new sediment P release risk index (SPRRI), Environ. Pollut., 255 (2019) 113279, doi: 10.1016/j.envpol.2019.113279.
[30] Y.N. Bai, X.N. Wang, J. Wu, Y.Z. Lu, L. Fu, F. Zhang, T.C. Lau, R.J. Zeng, Humic substances as electron acceptors for anaerobic oxidation of methane driven by ANME-2d, Water Res., 164 (2019) 114935, doi: 10.1016/J.WATRES.2019.114935.
[31] D.R. Lovley, J.D. Coates, E.L. Blunt-Harris, E.J.P. Phillips, J.C. Woodward, Humic substances as electron acceptors for microbial respiration, Nature, 382 (1996) 445–448.
[32] Q. Shen, C. Liu, Q. Zhou, J. Shang, L. Zhang, C.X. Fan, Effects of physical and chemical characteristics of surface sediments in the formation of shallow lake algae-induced black bloom, J. Environ. Sci. (China), 25 (2013) 2353–2360.
[33] K. Li, M. Yang, J. Peng, R. Liu, T.P. Joshi, Y. Bai, H. Liu, Rapid control of black and odorous substances from heavily-polluted sediment by oxidation: efficiency and effects, Front. Environ. Sci. Eng., 13 (2019), doi: 10.1007/s11783-019-1171-y.

Supplementary information

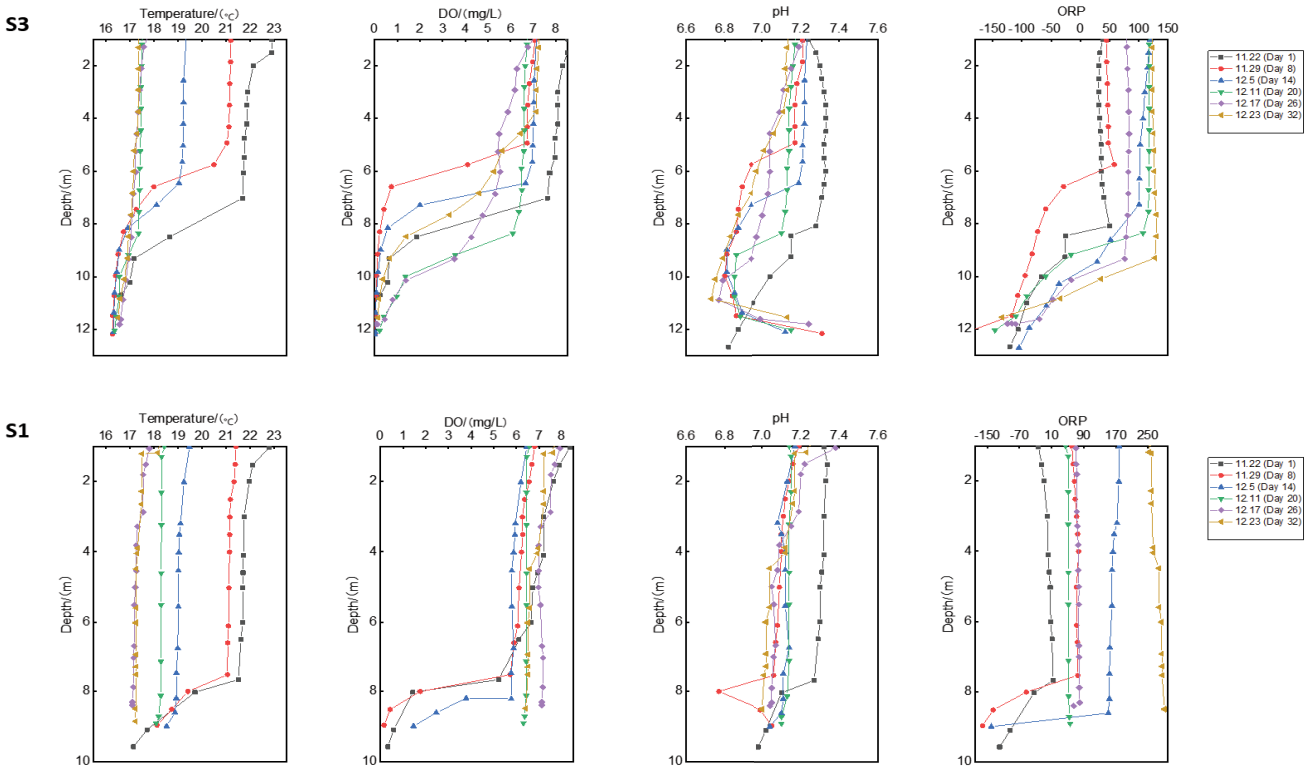

Fig. S1. Variation in water quality parameters (temperature, dissolved oxygen, pH, and oxidation–reduction potential) with depth at S3 and S1 in Tianbao Reservoir for days 1, 8, 14, 20, 26 and 32.

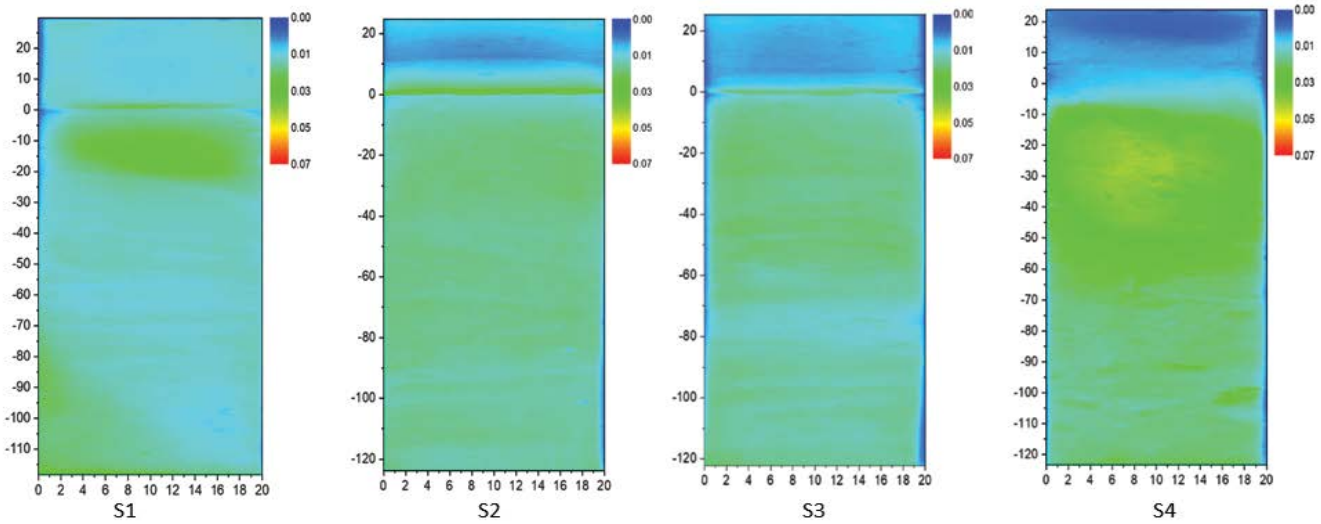

Fig. S2. High spatial resolution of 2D distribution of S^{2-} across the SWB at the various sampling sites.

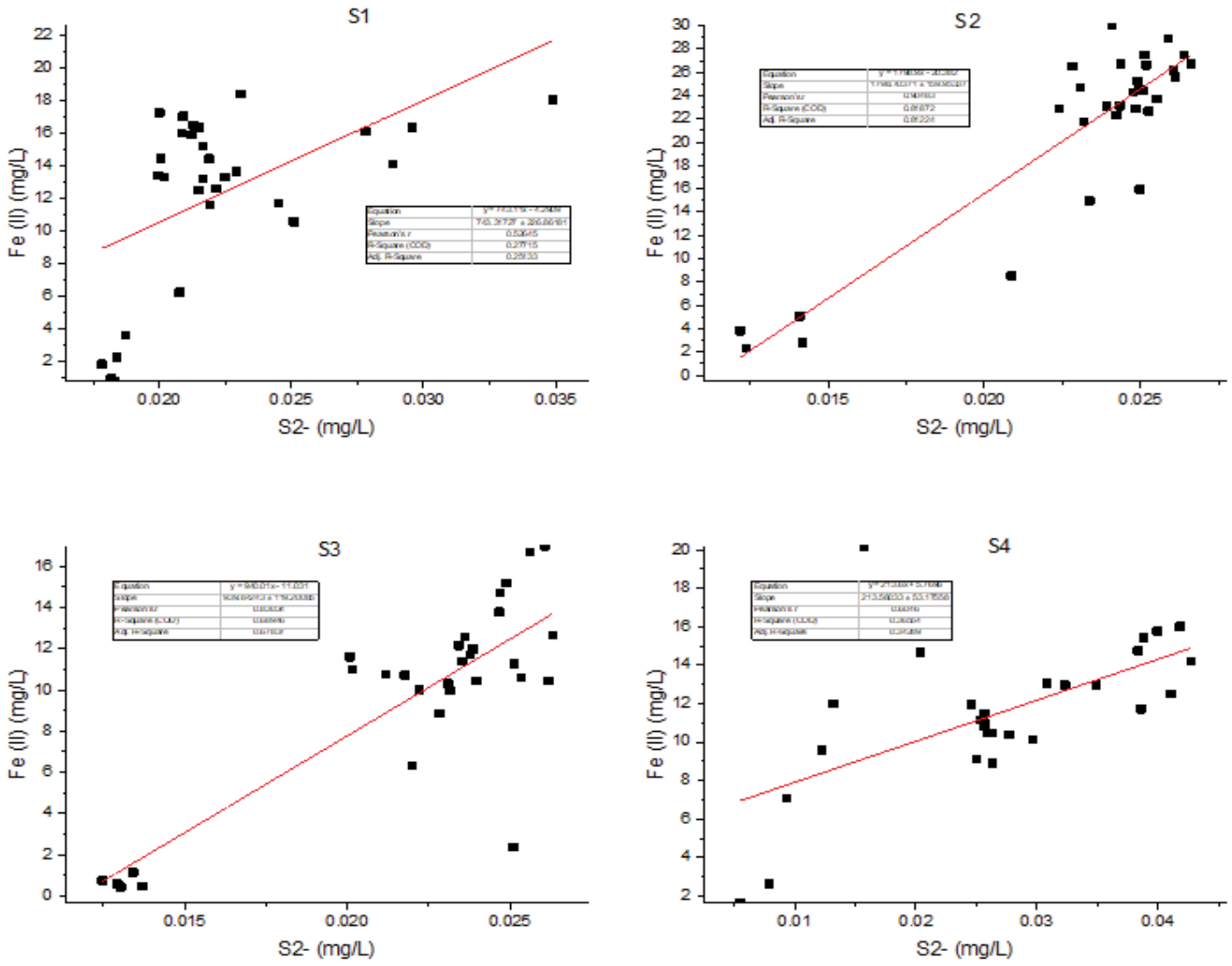

Fig. S3. Correlation between Fe^{2+} and S^{2-} at all sampling sites.

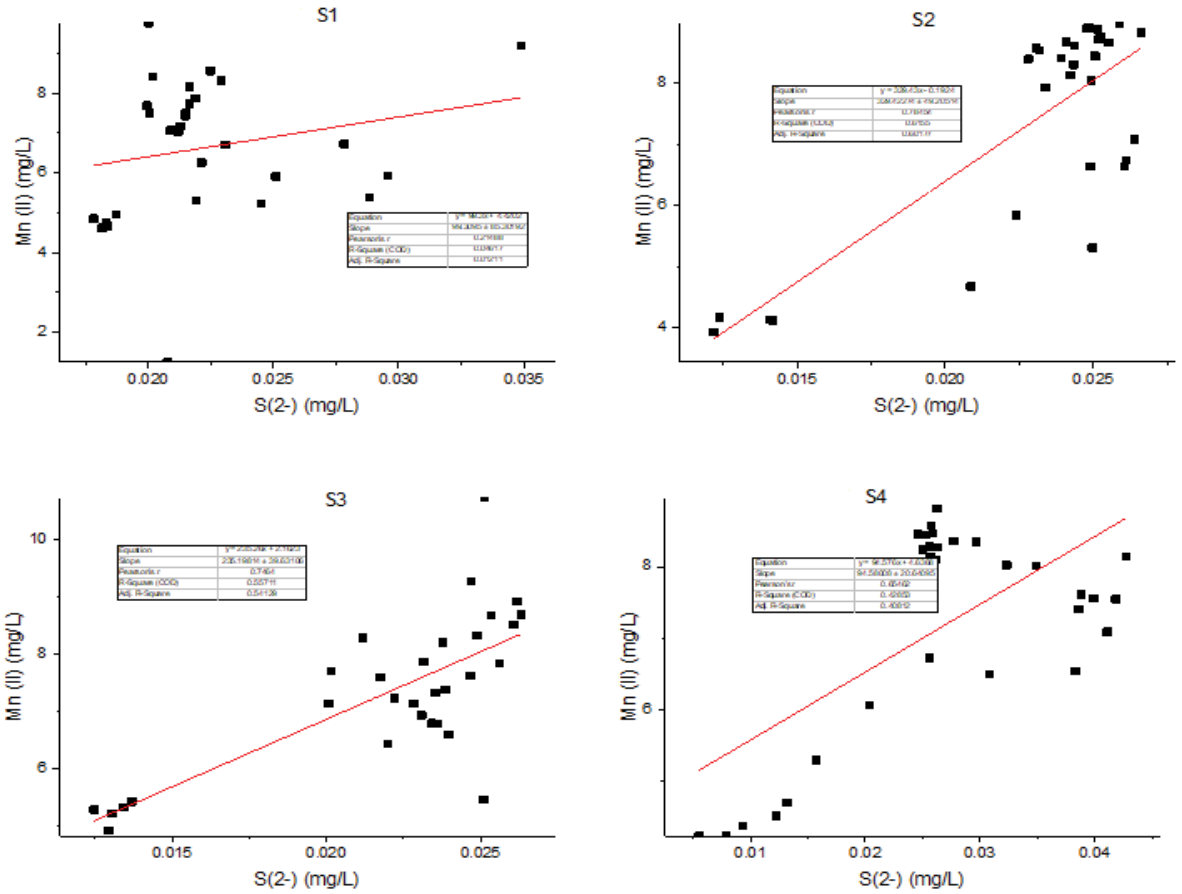

Fig. S4. Correlation between Mn^{2+} and S^{2-} at all sampling sites.

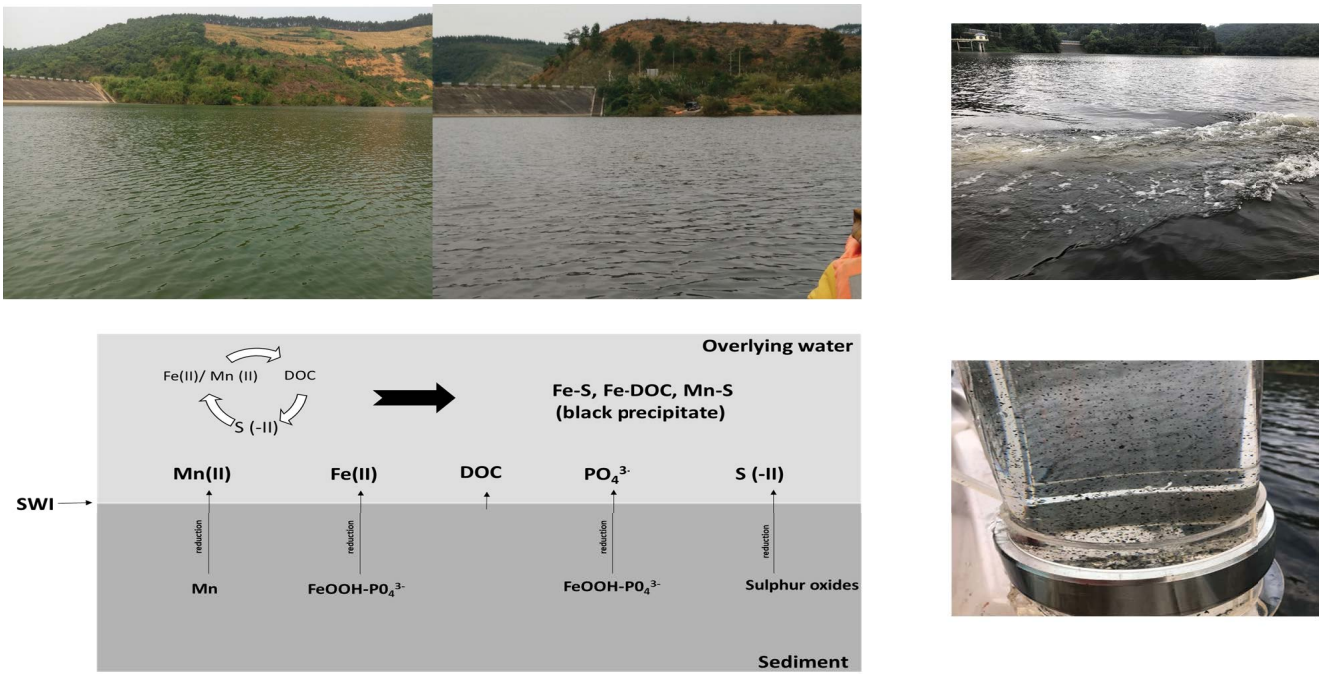

Fig. S5. Images of the black water in the Tianbao Reservoir, Southern China.